Ionospheric assimilation techniques for ARGOS Low-Resolution Airglow and Aurora Spectrograph (LORAAS) tomographically reconstructed equatorial electron density profiles

J. J. Sojka, J. V. Eccles, and R. W. Schunk

Space Environment Corporation, Providence, Utah, USA

S. McDonald, S. Thonnard, and K. Dymond

Naval Research Laboratory, Space Science Division, Washington, DC, USA

R. P. McCoy

Office of Naval Research, Arlington, Virginia, USA

Received 4 November 2002; revised 1 April 2003; accepted 8 May 2003; published 22 January 2004.

[1] The LORAAS instrument aboard the ARGOS satellite observes line-of-sight ultraviolet limb intensities from ionosphere and thermosphere airglow. This study uses tomographically reconstructed electron density profiles (EDPs) from the nightside emissions. The ionospheric reconstruction is performed using a two-dimensional O^+ 1356Å radiative recombination forward model and discrete inverse theory. The forward model assumes a Chapman layer for the vertical electron density distribution from which h_mF_2, N_mF_2, and topside scale height are derived for every 90 s limb scan, which is equivalent to 5° resolution in latitude. Since ARGOS is in a near Sun-synchronous orbit, these EDPs form a latitude slice through the equatorial anomaly structures at approximately 0230 LT. These data reflect ongoing ionospheric processes, and it is necessary to assimilate or compare with a model that contains appropriate ionospheric evolution such as the ionospheric forecast model (IFM). This study addresses the reasonableness of both the reconstructed EDPs and the IFM in describing the equatorial anomalies' diurnal and weather variability. The comparison of the LORASS EDPs with those of IFM for October 2000 show that the EDP reconstruction results compare favorably to the IFM EDPs in peak height and topside scale height. Additionally, the sector-to-sector climatology of the observed and modeled equatorial anomalies is similar to within the resolution of the instrument and model. The variability observed in each pass of the satellite is much larger than the IFM variability. The LORASS observation variability indicates that careful assessment of the representation error of the observations should be addressed through supplemental observations. *INDEX TERMS:* 2427 Ionosphere: Ionosphere/atmosphere interactions (0335); 2447 Ionosphere: Modeling and forecasting; 2415 Ionosphere: Equatorial ionosphere; *KEYWORDS:* ionosphere, data assimilation, airglow, modeling

Citation: Sojka, J. J., J. V. Eccles, R. W. Schunk, S. McDonald, S. E. Thonnard, K. Dymond, and R. P. McCoy (2004), Ionospheric assimilation techniques for ARGOS Low-Resolution Airglow and Aurora Spectrograph (LORAAS) tomographically reconstructed equatorial electron density profiles, *Radio Sci.*, *39*, RS1S07, doi:10.1029/2002RS002811.

1. Introduction

[2] The ARGOS satellite UV observations open the door to a long-awaited remote sensing capability. The unique attributes of these observations are that different wavelengths provide information on different parameters in the ionosphere-thermosphere (IT). Furthermore, these instruments are forerunners to instruments to be routinely flown on DMSP and NPOESS satellites. The UV observations at 1356 Å are the first to have been routinely processed and made available. These observations provide information

0048-6604/04/2002RS002811$11.00

on the nighttime O^+ electron density. This study has two objectives: first, to evaluate the final electron density profiles (EDP) from the tomographic inversion of the LORAAS observations through a direct comparison to the ionospheric forecast model (IFM) and second, to evaluate the climatological trends of the IFM through a comparison with LORAAS monthly average *F* region peak densities and heights.

[3] The IFM has been developed at Space Environment Corporation (SEC) as a physics-based ionospheric model [*Schunk et al.*, 1997]. It is also an element in the Global Assimilation of Ionospheric Measurements (GAIM) model [*Schunk et al.*, 2002]. Its role in GAIM is that of providing the first ionospheric density distribution from which Kalman-type assimilation will proceed. Hence the better this first specification is, the easier it will be for the Kalman procedures to generate a corrected and accurate ionospheric specification. This is accomplished by assimilating a wide range of observations, such as ionograms, total electron content (TEC) from GPS ground receivers, as well as GPS satellite occultations, DMSP satellite in situ plasma measurements, beacon satellite tomographic density slices, as well as future satellite UV IT parameters. Each data set must be validated and its accuracy defined and evaluated. Part of this accuracy determination is how well the measurement is representative of the entire ionospheric volume in which the measurement is made. In this usage, volume represents the altitude, latitude, and longitude bin in the assimilation model. This task is particularly difficult because, in this case, the latitude resolution of the observations is poorer than the resolution of potential assimilation models. In longitude they are comparable. In the nighttime equatorial anomaly region the role of the equatorial bubble phenomena is a major concern in determining the representation error because the first generation of ionospheric assimilation models will not include the equatorial bubble phenomena. An aspect of this study will be a discussion of the representation error.

[4] Section 2 gives an overview of the ARGOS satellite mission and its UV observations, while the specifics of the 1356 Å UV tomographic inversion to EDPs are given in section 3. The IFM is described in section 4. Section 5 provides the first LORAAS-IFM EDP comparisons for the month of October 2000. The results of these comparisons and their impact upon assimilation models is discussed and summarized in section 6.

2. ARGOS UV Observations

[5] The High-Resolution Airglow and Aurora Spectroscopy (HIRAAS) experiment was launched aboard the U.S. Air Force (USAF) Space Test Program's Advanced Research and Global Observation Satellite (ARGOS) on 23 February 1999. The satellite was placed into a Sun-synchronous orbit at 98° inclination at an altitude of approximately 830–850 km and a local time of 0230/1430. The HIRAAS consists of three limb scanning spectrographs shown in Table 1. The High-Resolution Ionospheric and Thermospheric Spectrograph (HITS) covers the far and extreme ultraviolet regime (500–1500 Å) in 120 Å segments with a 0.6–1.1 Å spectral resolution. The Ionospheric Spectroscopy and Atmospheric Chemistry (ISAAC) spectrograph covers the middle ultraviolet regime (1800–3200 Å) in 400 Å segments with a 3.8 Å spectral resolution. The Low-Resolution Airglow and Aurora Spectrograph (LORAAS) is an extreme and far ultraviolet spectrograph operating in the 800–1700 Å passband with an 18 Å spectral resolution. The HIRAAS instruments are described in more detail elsewhere [*Dymond and McCoy*, 1993; *McCoy et al.*, 1992, 1994].

Table 1. HIRAAS Instruments

Instrument	Passband	Spectral Resolution	Field of View
HITS	500–1800 Å	0.6–1.1 Å	4.6° × 0.06°
LORAAS	800–1750 Å	18.0 Å	2.4° × 0.15°
ISAAC	1800–3200 Å	3.8 Å	1.1° × 0.034°

[6] The LORAAS sensor is a prototype of the Special Sensor Ultraviolet Limb Imagers (SSULIs) that will fly on the USAF Defense Meteorological Satellite Program (DMSP) Block 5D-3 satellites in the 2002–2012 time frame. LORAAS views aft in the orbital plane and observes ultraviolet emissions on Earth's limb by scanning in the instrument's field-of-view from the satellite's local horizon to the edge of the hard disk. The instrument has a field-of-view of 2.4° × 0.15° and sweeps out a 2.4° × 17° field-of-regard during each 90 s scan, covering tangent altitudes of 750 km to 50 km. Approximately 90 spectra, with 1 s integration, are gathered per limb scan. When the flyback time is included, the instrument gathers a limb scan approximately every 5 to 6 degrees of latitude.

3. LORAAS EDPS

[7] We have used the LORAAS instrument to measure the intensity of the nighttime OI 1356 Å emission feature, which is produced primarily by radiative recombination. We assume the 1356 Å feature at night is optically thin and that contamination due to O^+-O^- neutralization is negligible [*Dymond and Thomas*, 2001].

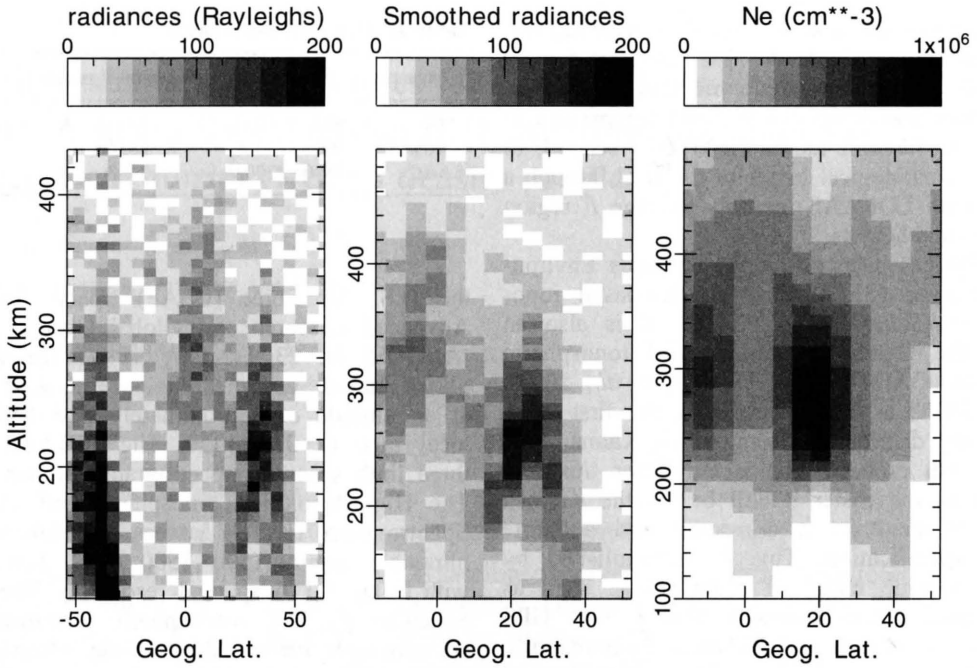

Figure 1. (left) Example of LORAAS EUV raw intensity image, (middle) smoothed intensity image, and (right) electron density reconstruction.

[8] The set of intensity profiles for a nighttime pass across the anomaly region can be represented as an image shown in Figure 1 (left panel). The image is a composite of 1356 Å intensity profiles, where the y axis represents the altitude in kilometers and the x axis represents the geographic latitude in degrees. The brightest features in the image are the aurora in the Southern Hemisphere and the equatorial anomaly. Figure 1 (center panel) shows the same intensity profiles with the aurora and noise removed and smoothed. Note that the geometry of the raw limb scans causes the anomalies to appear distorted.

[9] A quasi-tomographic technique is then used to invert the intensity scans to derive the electron density profiles of the F layer ionosphere in the equatorial anomaly region. The technique assumes a three parameter Chapman layer representation of the O^+ and electron density profiles [*Chamberlain and Hunten*, 1987]. The Chapman model uses three parameters to characterize the ionosphere: the peak density, N_mF_2; the height of the peak density, h_mF_2; and the O scale height, H_o, which is one-half the plasma scale height. The inversion algorithm is based on discrete inverse theory and uses the iterative Levenberg-Marquardt scheme to seek a maximum likelihood estimate (minimum of the chi-squared statistic) of the ionospheric parameters based on the fit of the model to the data [*Dymond and Thomas*, 2001]. Figure 1 (right panel) shows the two-dimensional (2-D) inversion of the intensity profiles shown in Figure 1 (center panel). The inversion properly removes the distortion caused by the geometry of the limb scans.

4. Ionospheric Forecast Model

[10] The IFM is a computationally robust physics-based computer code that could be run autonomously in a nonexpert weather specification and forecast facility. This model contains the key processes that occur in the terrestrial ionosphere and is driven by the dominant input mechanisms. Both the processes and inputs are discussed in detail by *Schunk* [1988] for the middle and high latitudes and by *Anderson* [1973] for the equatorial region. Mathematically, the IFM is a solution to the continuity, momentum, and energy equations for coupled pairs of major ions (NO^+ and O^+), minor molecular ions (O_2^+ and N_2^+), and the topside light ion H^+ determined analytically based on the O^+ profile. Ion production sources include photoionization, auroral ionization, and resonantly scattered solar radiation. Plasma transport is obtained from electric field models at both high and equatorial latitudes that augment corotation. Transport in the diffusion equation is associated with neutral winds and electric fields in regions where tilted magnetic

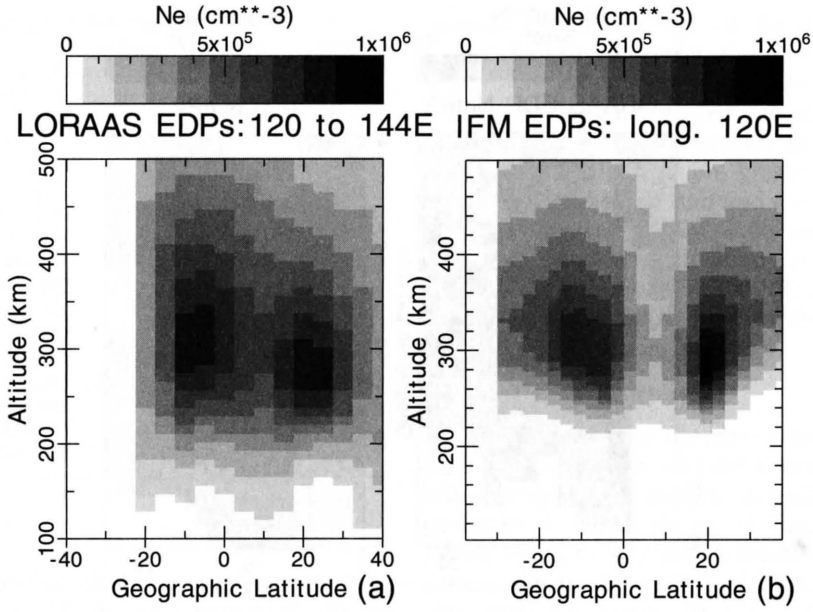

Figure 2. Electron density at 17.7 UT (120° to 144° east) based upon (a) LORAAS UV observations and from (b) IFM.

field lines cause vertical plasma transport. IFM is designed to be modular, which enables internal processes and inputs to be specified by a variety of source models either physical or empirical. Examples of the original modules are: neutral atmosphere is the MSIS-90 [*Hedin*, 1991]; high-latitude electric field [*Heppner and Maynard*, 1987]; equatorial electric field [*Scherliess and Fejer*, 1999]; auroral precipitation [*Hardy et al.*, 1985]; and neutral wind [*Hedin et al.*, 1991]. The advantage of the modular design is that as those modules (input models) are updated and improved, they are readily incorporated in the IFM. Indeed, the present-day version of IFM has various updated modules. The IFM was developed by SEC for the U.S. Air Force [*Schunk and Sojka*, 1994].

[11] A major aspect of developing any model is its validation. In the case of IFM, its developers had decades of experience in ionospheric physics both theoretically [*Schunk*, 1988] and with model validation [*Sojka*, 1989]. This aspect of the IFM development has been continuous at SEC [*Schunk et al.*, 1997]. The IFM has also been used as a test bed for data assimilation experiments. Midlatitude observations at Puerto Rico (specifically, ionosonde, incoherent scatter radar, and GPS total electron content (TEC) measurements) have been used in assimilation-validation studies. Modified versions of the IFM were developed to assimilate these data types in order to demonstrate the real time specification advantages associated with assimilation techniques [*Sojka et al.*, 2001]. The IFM model also plays the crucial "first step" in the global assimilation of ionospheric measurements (GAIM) [*Schunk et al.*, 2002].

5. LORAAS-IFM EDP Comparisons

[12] The period for this comparison is the entire month of October 2000. During the month, there were 4 days whose average 3-hourly *Kp* index was 4 or larger. These have been removed from the data sets presented as average October 2000 observations because they are noticeably disturbed. The remaining 27 days had an average 3-hourly *Kp* of 2.0. The LORAAS data consists of 14 orbits per day in the 0230 LT sector. In order to produce monthly averages of the EDPs, these orbits were binned into 15 geographic longitude bins each 24° wide. These longitude sectors were further binned into 5° wide geographic latitude bins. In altitude, the EDPs have a resolution of 9 km.

[13] The IFM output was rebinned to provide densities on similar spatial resolution. A longitude bin was selected from 48, 7.5° geographic longitude resolution slices, and each of these IFM slices has a 3° geographic latitude resolution. In altitude, the IFM profiles were stored at variable resolution. For specific EDP comparisons the IFM profiles have been interpolated on a logarithmic density scale to 5 km steps to be more comparable with the LORAAS EDPs.

5.1. EDPs at 1830 UT

[14] Figure 2a shows the LORAAS 27-day average distribution of the equatorial anomaly at 1830 UT as

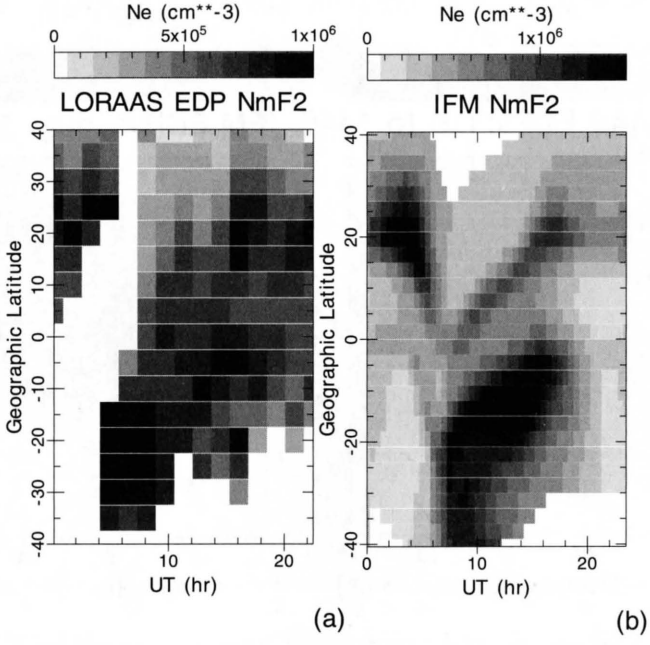

Figure 3. N_mF_2 as a function of UT and geographic latitude from (a) LORAAS EDPs and (b) IFM. White regions indicate "no data" in Figure 3a and "no values" in Figure 3b.

contours of electron density. In this figure, both anomalies can be identified. The southern anomaly has a peak density of 7.5×10^5 cm^{-3} at an altitude of 310 km and a geographic latitude of $-8°$. Its northern anomaly has a density of 8×10^5 cm^{-3} but is lower at 280 km and a geographic latitude of 22°.

[15] Figure 2b is the IFM slice at 1830 UT that corresponds to the Figure 2a ARGOS satellite pass. The ionospheric-thermospheric conditions corresponded to an F10.7 solar radio flux index of 171, a mean F10.7 of 149, and a daily ap of 2. In this simulation the equatorial vertical drift model of *Scherliess and Fejer* [1999] has been used. The IFM simulation results show two well-defined anomaly peaks. The southern anomaly has a peak density of 7×10^5 cm^{-3}, a height of 305 km, and is located at $-7°$ geographic latitude, while the northern peak has a density of 9×10^5 cm^{-3}, a height of 290 km, and at a geographic latitude of 20°.

[16] This initial comparison is very encouraging. The anomaly north south asymmetry is very similar in both observation and model, with the northern anomaly being lower in altitude and higher in density. There are differences, especially in the bottom side, in which the IFM profiles have a sharp drop-off while the LORAAS reconstructed Chapman bottom side extends to below 200 km.

5.2. N_mF_2 UT Morphology

[17] Figure 3a is a contour plot of the LORAAS EDP peak density, N_mF_2, as a function of UT (longitude) and geographic latitude. The UT represents the daily orbital sequence of ARGOS passes through the night 0230 LT sector. Table 2 provides the relationship between these UTs and corresponding longitude bins. This figure shows how the location of the anomalies is associated with the variation of the magnetic equator rather than the geographic equator. Also present in Figure 3a is a region from 0000 to 0500 UT from $-40°$ to almost 20° where the ARGOS satellite and the LORAAS instrument are adversely affected by the South Atlantic Anomaly (SAA). This anomaly is independent of the ionosphere; in fact, it is a high-radiation dosage region that causes noise in the satellite electronics and high backgrounds in sensors. At this time the SAA region, in Figure 3a, is set to zero to avoid making complex corrections to the observations. Between 0500 and 1500 UT the southern F region anomaly dominates with almost no northern one being present. Between 1630 and 2200 UT, both anomalies are clearly evident, while from 0000 to 0500 UT a clear strong northern anomaly is present. Note this latter lack of a southern anomaly could simply be due to the SAA missing data. The observations show a well-defined anomaly UT (longitude) dependence.

[18] Figure 3b shows the corresponding IFM N_mF_2 distribution using the October 2000 average conditions simulation as described for Figure 2b. The white area on Figure 3b indicates where the low-latitude portion of IFM has not calculated an electron profile. Between 0700 and 1600 UT the southern anomaly is dominant and

Table 2. Mean UT for ARGOS Longitude Bins

Bin	Geographic Longitude, deg	Mean Hours, UT
1	0–24	1.7
2	24–48	0.1
3	48–72	22.5
4	72–96	20.9
5	96–120	19.3
6	120–144	17.7
7	144–168	16.1
8	168–192	14.5
9	192–216	12.9
10	216–240	11.3
11	240–264	9.7
12	264–288	8.1
13	288–312	6.5
14	312–336	4.9
15	336–360	3.3

much broader in latitude than the northern anomaly. From 1600 to 2000 UT the two anomalies are of comparable densities, while from 2000 UT to 0600 UT the northern anomaly dominates with almost no significant southern anomaly.

[19] The comparison between Figures 3a and 3b is very encouraging. Both the anomaly UT morphology in geographic latitude of the peaks as well as their densities are close enough that they represent the same phenomena. The model simulation predicts the northern anomaly between 0700 and 1400 UT to be very narrow; in fact, it is probably narrower than the 5° LORAAS resolution, which may be the reason why the LORAAS averaged EDPs only show the southern anomaly during this time interval. The southern anomaly is very broad both in observation and simulation; greater than 10°. Both the observation and simulation find the northern anomaly to be very distinct between 1600 and 1800 UT at 20° geographic latitude. Although the northern anomaly comparison between 0000 and 0500 UT is encouraging, the effect of the SAA prevents the southern anomaly comparison from being made.

5.3. h_mF_2 UT Morphology

[20] Figures 4a and 4b present the h_mF_2 distributions from LORAAS EDP and those from IFM simulations, respectively. They are the complementary F region parameter to N_mF_2 shown in Figures 3a and 3b. In Figure 4a the missing data in the 0000 to 0500 UT sector corresponds to SAA-affected measurements that have been excluded. Figure 4b IFM h_mF_2 are shown at the 20 km resolution of the IFM output database.

[21] In order to discuss the anomaly peak height associated with the northern and southern anomaly, it is necessary to refer also to Figures 3a and 3b for the locations of the anomaly peak densities. The LORAAS EDPs show that the southern anomaly is dominant from 0500 to 1500 UT, and from Figure 4a it has an altitude ranging from 280 to 380 km. However, the northern

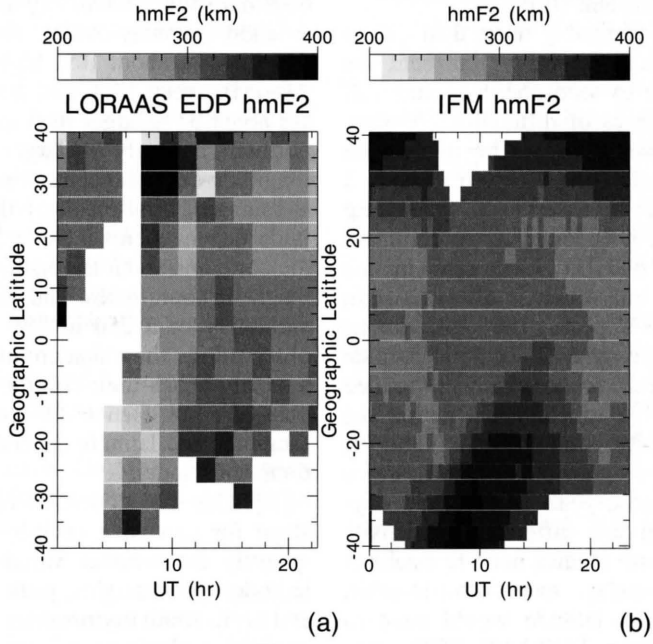

Figure 4. Here h_mF_2 is shown as a function of UT and geographic latitude from (a) LORAAS EDPs and (b) IFM. White regions indicate "no data" in Figure 4a and "no values" in Figure 4b.

anomaly is lower at all UTs ranging from 270 to 300 km. The IFM simulation has a similar altitude asymmetry. Figure 4b shows that the 0600 to 1500 UT southern dominant anomaly lies in the altitude range 320 to 370 km and that the northern anomaly lies lower from 280 to 320 km. Noticeably, both the observations and simulations have the highest h_mF_2 and largest N_mF_2 values in the southern anomaly between 0600 and 1500 UT.

6. Assimilation: Considerations and Cautions

[22] The GAIM data assimilation model uses the IFM as the climatology background and when improved drivers are available to use IFM to improve on climatology. Figures 3b and 4b show this IFM climatology for the N_mF_2 and h_mF_2 parameters. Apart from the 3° latitude and half-hour UT model resolution, these two distributions are smoothly varying. They lack weather variability. For data assimilation modeling, it is important to account for the weather dynamic range as part of the representativeness error associated with the observations. The observations being presented in Figures 3a and 3b are electron density profile peak height and densities from an inversion of LORAAS optical observations. Neither the observed N_mF_2 nor h_mF_2 are smooth, yet they represent the average over 27 days. The high degree of variability is present from one orbit to the next (the vertical stripes of Figures 3a and 4a) as well as from one latitude bin to the next (horizontal stripes).

[23] This variability is considerably more than due to counting statistics. Does this variability represent the representativeness error due to ionospheric weather? If not, what are the other sources of difference? A more extensive day-by-day analysis needs to be undertaken to attempt to extract this information. From Figures 3 and 4 a number of facts can be ascertained. Beginning with the southern anomaly, it is found to be dominant between about 0700 and 1600 UT. Each orbit in this period has a peak latitude bin which is always within ±1 bin of the IFM model's peak. The observations show the peak to be spread over 2–3° or 5° in latitude bins, whereas the IFM tends to have a well-defined peak latitude. Over this 0700 to 1600 UT period the maximum peak model density is about 35% higher. If the 27-day averaging was responsible for smearing a narrower peak structure whose peak latitude had day-to-day variability ±5°, then this difference in density would be expected. Follow-up studies need to establish this. Such a strong day-to-day, even orbit-to-orbit, motion of the anomaly peak latitude would need to be included in GAIM. These LORAAS EDPs may well provide a means of quantifying this dynamics for GAIM on a 90 min orbital timescale.

[24] The other aspect of the representation error is accounting for model observation differences caused by processes missing from the model. Perhaps the most fundamental missing process that affects nighttime equatorial plasma density is the ionospheric irregularity process in which bubbles of rarified plasma reduce density along flux tubes by over an order of magnitude. These bubbles would have dimensions that extend over many altitude and latitude bins but probably are restricted to a longitude sector (bin). Hence, are these possible localized plasma depletions the cause of the large variability found in the 27-day averages shown in Figure 3a? If the presence of bubbles is the cause, then the assigned representation error must be increased prior to proper assimilation into GAIM, which does not include plasma bubble physics. If sector-to-sector variability in the vertical drift history prior to the LORAAS pass is the cause of the observed variability, then GAIM would contain the physics necessary and greater weight can be given to the observation in the assimilation procedure. Future work needs to find alternative observations to determine if and when bubbles are present so that a correct interpretation of the representation error can be made. This "bubble identification" is a major objective of the Communication/Navigation Outage Forecast System (C/NOFS) satellite mission.

[25] Over the same 0700 to 1600 UT period the northern anomaly is less evident. The IFM peak density shows it as a narrow <5° structure. This is sub-LORAAS latitude bin size. In fact, the LORAAS N_mF_2 (Figure 3a) does not show an anomaly as such. Numerically, there is a slight anomaly which shows that the model peak densities are about 10% higher.

[26] Between 1700 and 2400 UT the LORAAS N_mF_2 are about 35% larger than the IFM values, but now the northern anomaly is larger. That the model diurnal, longitude-dependence, is observed (even if crudely) is an encouraging first result of the comparison. Other longitude dependencies include the geographic locations of the north and south anomalies which are primarily tied to magnetic coordinates. The peak heights are also showing variability of a 250 to 350 km range. The model and observations show that around the northern and southern anomaly peaks their altitude difference tends to be less than ±20 km. Hence the layer is showing very similar longitude and latitude dependencies in both the observations and model.

[27] This first LORAAS EDP model study has set the stage for extensive orbit-by-orbit analysis in order to quantify the weather variability of the anomaly peak latitudes, peak heights, peak densities, as well as widths and north-south asymmetries. Such information will help establish realistic covariance matrices for Kalman filters that assimilate observations with models of the equatorial ionosphere. These analyses may well provide a method

for obtaining equatorial electric field and cross-equator neutral wind drivers based on the anomaly latitude separation observed in each orbit.

[28] From even this relatively simple first study, the variability from day-to-day or orbit-to-orbit is inferred to be "large." A major contribution from even simple LORAAS EDP analysis will be the quantification of this variability. However, to resolve the issue of the contribution of *F* region irregularities to the variability observed from orbit to orbit, it will be necessary to have additional data. Our future plans include using the C/NOFS near-equatorial orbit measurements to determine how much the irregularities contribute to the mean density of the ionospheric volume as inferred from the LORAAS UV observations. The C/NOFS plasma measurements are made on spatial scales at least 100 times smaller than the UV volume measurement. A statistical study of the C/NOFS data to define the effect of irregularity depletions on background ionosphere density will determine the representation error of the UV observations for the first generation GAIM-type models that lack plasma bubble physics.

[29] **Acknowledgments.** This work was supported by contract N00014-98-C-0085 from the Office of Naval Research to Space Environment Corporation. The Naval Research Laboratory work was supported by the Office of Naval Research.

References

Anderson, D. N. (1973), A theoretical study of the ionospheric F region equatorial anomaly, I. theory, *Planet. Space Sci.*, *21*, 409–419.

Chamberlain, J. W., and D. M. Hunten (1987), *Theory of Planetary Atmospheres: An Introduction to Their Physics and Chemistry*, Academic, San Diego, Calif.

Dymond, K. F., and R. P. McCoy (1993), Ultraviolet spectrographs for thermospheric and ionospheric remote sensing, *Proc. SPIE Int. Soc. Opt. Eng.*, *I940*, 117–127.

Dymond, K. F., and R. J. Thomas (2001), An algorithm for inferring the two-dimensional structure of the nighttime ionosphere from radiative recombination measurements, *Radio Sci.*, *36*, 1241–1254.

Hardy, D. A., M. S. Gussenhoven, and E. Holeman (1985), A statistical model of auroral electron precipitation, *J. Geophys. Res.*, *90*, 4229–4248.

Hedin, A. E. (1991), Extension of the MSIS thermosphere model into the middle and lower atmosphere, *J. Geophys. Res.*, *96*, 1159–1172.

Hedin, A. E., et al. (1991), Revised global model of thermospheric winds using satellite and ground-based observations, *J. Geophys. Res.*, *96*, 7657–7688.

Heppner, J. R., and N. C. Maynard (1987), Empirical high-latitude electric field models, *J. Geophys. Res.*, *92*, 4467–4489.

McCoy, R. P., K. F. Dymond, G. G. Fritz, S. E. Thonnard, R. R. Meier, and P. A. Regeon (1992), Far- and extreme-ultraviolet limb imaging spectrograph for the DMSP satellites, *Proc. SPIE Int. Soc. Opt. Eng.*, *1745*, 310–321.

McCoy, R. P., K. F. Dymond, G. G. Fritz, S. E. Thonnard, R. R. Meier, and P. A. Regeon (1994), Special Sensor Ultraviolet Limb Imager: An ionospheric and neutral density profiler for the Defense Meteorological Satellite Program satellites, *Opt. Eng.*, *33*, 423–429.

Scherliess, L., and B. Fejer (1999), Radar and satellite global equatorial F region vertical drift model, *J. Geophys. Res.*, *104*, 6829–6842.

Schunk, R. W. (1988), A mathematical model of the middle and high latitude ionosphere, *Pure Appl. Geophys.*, *127*, 255–303.

Schunk, R. W., and J. J. Sojka (1994), Development of a global ionospheric forecast model, *Rep. PL-TR-94-2232*, Phillips Lab., Directorate of Geophys., Hanscom AFB.

Schunk, R. W., J. J. Sojka, and J. V. Eccles (1997), Expanded capabilities for the ionospheric forecast model, *Rep. AFRL-VS-HA-TR-98-0001*, Air Force Res. Lab., Space Vehicles Directorate, Hanscom AFB.

Schunk, R. W., et al. (2002), Global Assimilation of Ionospheric Measurements (GAIM), in *Proceedings of the 2002 Ionospheric Effects Symposium*, edited by J. M. Goodman, pp. 50–61, Off. of Nav. Res., Arlington, Va. (Available as PB2003-104280 from www.ntis.gov)

Sojka, J. J. (1989), Global scale, physical models of the *F* region ionosphere, *Rev. Geophys.*, *27*, 371–403.

Sojka, J. J., D. C. Thompson, R. W. Schunk, T. W. Bullett, and J. J. Makela (2001), Assimilation Ionosphere Model: Development and testing with Combined Ionospheric Campaign Caribbean measurements, *Radio Sci.*, *36*, 247–259.

K. Dymond, S. McDonald, and S. Thonnard, Naval Research Laboratory, Space Science Division, 4555 Overlook Ave., Washington, DC 20375, USA.

J. V. Eccles, R. W. Schunk, and J. J. Sojka, Space Environment Corporation, 221 N. Spring Creek Parkway, Suite A, Providence, UT 84332, USA. (vince.eccles@spacenv.com)

R. P. McCoy, Office of Naval Research, 800 N. Quincy Street, Arlington, VA 22217-5660, USA.